Bull. Astr. Soc. India (2014) **42**, 101–119

The Double Pulsar J0737−3039A/B: a decade of surprises

M. Burgay[1]*, M. Kramer[2,3] and M. A. McLaughlin[4]

[1]*INAF - Osservatorio Astronomico di Cagliari, via della Scienza 5, 09047 Selargus (CA), Italy*
[2]*Max-Planck-Institut fÃijr Radioastronomie, Auf dem HÃijgel 69, 53121 Bonn, Germany*
[3]*Jodrell Bank Centre for Astrophysics, University of Manchester, Alan-Turing-Building, Manchester M13 9PL, UK*
[4]*Department of Physics and Astronomy, West Virginia University, Morgantown, WV 26506, USA*

Received 2014 September 26; accepted 2014 November 04

Abstract. The Double Pulsar J0737−3039A/B, discovered with the Parkes radio telescope in 2003, is one of the most intriguing pulsar discoveries of the last decade. With its orbital velocity of ∼1% of the speed of light, it is the most relativistic system ever found and, thanks to the presence of *two* active radio pulsars, it has also shown unprecedented mutual interactions between the radio beam of one pulsar and the magnetosphere of the other. Due to these characteristics, the Double Pulsar can be used for a wide variety of experiments, ranging from relativistic gravity, to plasma physics, and to pulsar electrodynamics. Moreover its discovery enhances – by almost an order of magnitude – estimates of merger rates for double neutron stars systems, providing new possibilities for the current generation of ground-based gravitational wave detectors. In this paper we review the main observational properties of the Double Pulsar and their application for physical and astrophysical studies.

Keywords : neutron star, pulsar, J0737−3039A/B, relativity

1. Introduction

The Double Pulsar system J0737−3039A/B (Burgay et al. 2003; Lyne et al. 2004) was discovered during the 20-cm Parkes High-latitude pulsar survey (Burgay et al. 2006) and its follow-up observations. The first pulsar of the binary system to be detected, J0737−3039A (in the following 'A'; Fig. 1 left) is a mildly recycled 22.7 ms pulsar. Its orbital parameters, implying an orbital velocity of about 1% of the speed of light, together with a remarkably high value of the periastron

*email: burgay@oa-cagliari.inaf.it

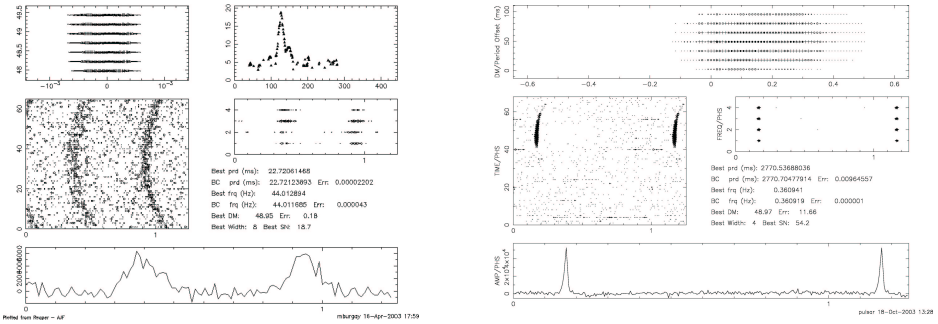

Figure 1. Original discovery plots for pulsar A (left) and pulsar B (right) of the Double Pulsar. Bottom panel shows the integrated pulse profile (over 4 minutes for A and 53 minutes for B) of the two pulsars. Above, on the left, the folded profile is represented in a grey-scale as a function of time over 64 time sub-integrations. For pulsar A the drift in phase due to orbital motion is clearly visible, while for pulsar B we can see the pulse appearing around subintegration 40 and disappearing around 60. In the centre, to the right, the pulsars signal folded in phase is shown as a function of the observing frequency, split in four frequency sub-bands. On the top-left a grey-scale of the signal-to-noise of the integrated pulse profile is plotted as a function of varying spin period and dispersion measure (DM). For pulsar A, on the top-right, the intensity of the signal is plotted against the DM trial values of the blind search for pulsed signals applied to the Parkes High-latitude data. This plot is missing for pulsar B, as the DM was already known.

advance ($\dot{\omega}$ = 16.9 deg/yr), identified it immediately as a member of the most extreme relativistic binary system ever discovered. From the compactness of the system one can also derive a very small merging timescale (T_{merge} = 85 Myr) which, leads to an increase of the estimates on the double neutron star coalescence rate (Burgay et al. 2003; Kalogera et al. 2004a,b; O'Shaughnessy & Kim 2010), improving the probability of detecting merging neutron stars (NSs) with ground-based gravitational wave detectors.

A few months after its discovery, analysis of follow-up observations of pulsar A led to the discovery of a second pulsar in the system (Lyne et al. 2004), the 2.8-s pulsar J0737−3039B (hereafter 'B'; Fig 1, right). Pulsar B was not detected earlier because, unexpectedly, this object was bright only in two short segments of the orbit; for the rest of the time its pulsed signal is very week or absent.

Upon close inspection, the pulsed signals of both pulsar A and pulsar B revealed several other intriguing characteristics. Pulsar A is eclipsed for about 30 s near superior conjunction, with its eclipse being modulated at half of pulsar B's period; pulsar B shows orbital-dependent variations not only in its flux, but also in its pulse shape (Lyne et al. 2004). Variations of the pulse shape on longer timescales and variations of the extent and location of B's bright phases are also observed (Burgay et al. 2005; Perera et al. 2010). Finally, features similar to drifting subpulses (e.g. Lorimer & Kramer 2005) that are spaced by exactly the period of the A pulsar are seen in B's single pulses (McLaughlin et al. 2004a). All these peculiar phenomena can be ascribed to interactions between the emission beam of one pulsar and the magnetosphere of the other. Their variation in time likely depends on the fact that the geometry of the system, and

hence our viewing angle towards it, is changing in time due to relativistic spin precession. In the Double Pulsar this relativistic effect happens on such a short timescale (75 and 71 years for pulsars A and B, respectively) that, besides making all the aforementioned variations detectable over a very short timescale, it led pulsar B's beam to become undetectable in 2008 (Perera et al. 2010).

In this contribution we review the history and most important results on J0737−3039A/B and their applications for various physical and astrophysical studies. In particular, in section §2 we describe the experiments related to testing relativistic gravity in the strong field regime (general relativity, §2.1, and alternative theories, §2.2), in §3 we report on the impact of the Double Pulsar discovery on the detectability of gravitational waves caused by double neutron star mergers, and in §4 we describe the applications to magnetospheric, pulsar electrodynamics, and plasma physic studies from the observational signatures of interactions in the system. Finally in §5 we present some possible future applications.

2. Testing relativistic gravity with the Double Pulsar

After the discovery of a pulsar, in order to fully exploit its potential as an astrophysical laboratory, it is necessary to start a follow-up campaign of observations to precisely measure its spin, astrometric and, in case of a binary system, orbital parameters. This is done through *pulsar timing*, a technique that allows to precisely measure the times of arrival (ToA) of the pulses. These are then compared with ToA predicted by a given pulsar model. The best fit positional, rotational, and orbital parameters are then obtained through minimizing the differences, or timing residuals, between measured and predicted ToA with a multiparametric fit (see e.g. Lorimer & Kramer 2005).

Because of their strong gravitational fields and fast orbital motions, binary systems containing two neutron stars can exhibit large relativistic effects (Damour & Deruelle 1986). If one (or two, as in this unique case) of the NSs emits regular pulsed signals, it is possible, through pulsar timing, to measure directly not only the spin, astrometric, and Keplerian orbital parameters, but also the relativistic corrections to the Keplerian description of the orbit, or the so called "post-Keplerian" (PK) parameters. These accurate measurements allow to test relativistic gravity. For point masses with negligible spin contributions, the PK parameters can be written as a function of the masses of the two stars in the system and of the (measured) Keplerian parameters. With the two masses as the only unknowns, the measurement of n (with $n \geq 3$) PK parameters over-constrains the system, hence providing $n - 2$ tests for the chosen theory of gravity (Damour & Taylor 1992).

Graphically these tests are usually represented through a mass-mass diagram, with the mass of the pulsar on the x-axis and the mass of the companion on the y-axis, in which all the observational constraints on the masses of the system can be plotted. The first such constraint, purely Newtonian, is given by the pulsar mass function, simply imposing that $sin(i)$ (with i the inclination of the orbit) cannot be greater than one. This will exclude all the values for the masses

below the mass-function curve. Every PK parameter measured can be translated in a curve (or rather, in a pair of curves encompassing the PK value and its error) on the mass-mass diagram; two PK parameters will define an area in the plot (and a value, with its error, for the two masses separately) and the pair of curves for any further PK parameter measured will have to overlap to this area for the theory to pass the test. This approach has the additional benefit of narrowing the range of allowed masses dramatically.

2.1 General Relativity

Timing parameters, including PK parameters, for the Double Pulsar are listed in Table 1.

For general relativity (GR) the equations describing the five most used PK parameters can be written (to lowest Post-Newtonian order) as (Damour & Deruelle 1986; Taylor & Weisberg 1989; Damour & Taylor 1992):

$$
\begin{aligned}
\dot{\omega} &= 3T_{\odot}^{2/3}\left(\frac{P_b}{2\pi}\right)^{-5/3}\frac{1}{1-e^2}\,(M_A+M_B)^{2/3},\\
\gamma &= T_{\odot}^{2/3}\left(\frac{P_b}{2\pi}\right)^{1/3} e\,\frac{M_B(M_A+2M_B)}{(M_A+M_B)^{4/3}},\\
\dot{P}_b &= -\frac{192\pi}{5}T_{\odot}^{5/3}\left(\frac{P_b}{2\pi}\right)^{-5/3}\frac{\left(1+\frac{73}{24}e^2+\frac{37}{96}e^4\right)}{(1-e^2)^{7/2}}\frac{M_A M_B}{(M_A+M_B)^{1/3}},\\
r &= T_{\odot}M_B,\\
s &= T_{\odot}^{-1/3}\left(\frac{P_b}{2\pi}\right)^{-2/3} x\,\frac{(M_A+M_B)^{2/3}}{M_B},
\end{aligned}
$$

where P_b is the orbital period, e the eccentricity and $x = asini$ the projected semi-major axis of the orbit measured in light-s. The masses M_A and M_B of A and B respectively (or, in general, of the pulsar and its companion), are expressed in solar masses. The constant $T_{\odot}$ is defined as $T_{\odot} = GM_{\odot}/c^3 = 4.925490947\mu$s where G is the Newtonian constant of gravity and c the speed of light. The PK parameter $\dot{\omega}$ is phenomenologically associated with the advance of the periastron, γ accounts for gravitational red-shift and time dilation, $\dot{P}_b$ is the orbital damping and, in the framework of general relativity, measures the rate at which the orbital period decreases due to emission of gravitational radiation. Finally, r and $s \equiv \sin i$ represent, respectively, the rate and the shape of the Shapiro delay (Shapiro 1964), or the time delay of the radio signal caused by the space-time deformations around the companion star.

Already after just three years of pulsar timing, the Double Pulsar yielded precise measurements of all five PK parameters. For this system and for this system only, moreover, due to the presence of *two* active pulsars, it has also been possible to obtain a further, *theory independent* constraint on the masses. The ratio between the two projected semimajor axes $R = x_B/x_A$ can

Table 1. Values in table were derived from timing observations presented in Kramer et al. (2006). The positional parameters are in the DE405 reference frame. Time dependent values are in barycentric dynamical time (TDB) units at the timing epoch quoted in Modified Julian Days (MJDs). The Keplerian binary parameters (P_b, e, ω, T_0, and x) are derived from timing of pulsar A. The first four of these (with an offset of 180 ° added to ω) and the position parameters were held fixed when fitting for B's parameters. The dispersion-based distance is obtained assuming the Cordes & Lazio (2002) model for the interstellar electron density.

Timing parameter	**PSR J0737−3039A**	**PSR J0737−3039B**
Right Ascension α	$07^{\rm h}37^{\rm m}51^{\rm s}.24927(3)$[a]	–
Declination δ	$-30°39'40''.7195(5)$	–
Proper motion in the RA direction (mas yr^{-1})	−3.3(4)	–
Proper motion in Declination (mas yr^{-1})	2.6(5)	–
Parallax, π (mas)	3(2)	–
Spin frequency ν (Hz)	44.054069392744(2)	0.36056035506(1)
Spin frequency derivative $\dot{\nu}$ (s^{-2})	$-3.4156(1) \times 10^{-15}$	$-0.116(1) \times 10^{-15}$
Timing Epoch (MJD)	53156.0	53156.0
Dispersion measure DM (cm^{-3}pc)	48.920(5)	–
Orbital period P_b (day)	0.10225156248(5)	–
Eccentricity e	0.0877775(9)	–
Projected semi-major axis $x = (a/c)\sin i$ (s)	1.415032(1)	1.5161(16)
Longitude of periastron ω (deg)	87.0331(8)	87.0331 + 180.0
Epoch of periastron T_0 (MJD)	53155.9074280(2)	–
Advance of periastron $\dot{\omega}$ (deg/yr)	16.89947(68)	[16.96(5)][b]
Gravitational redshift parameter γ (ms)	0.3856(26)	–
Shapiro delay parameter s	0.99974(−39, +16)	–
Shapiro delay parameter r (μs)	6.21(33)	–
Orbital period derivative $\dot{P}_b$	$-1.252(17) \times 10^{-12}$	–
Total proper motion (mas yr^{-1})	4.2(4)	
Distance d(DM) (pc)	∼500	
Distance $d(\pi)$ (pc)	200 − 1000	
Transverse velocity (d = 500 pc) (km s^{-1})	10(1)	
Orbital inclination angle (deg)	88.69(-76,+50)	
Mass function ($M_\odot$)	0.29096571(87)	0.3579(11)
Mass ratio, R	1.0714(11)	
Total system mass ($M_\odot$)	2.58708(16)	
Neutron star mass ($m_\odot$)	1.3381(7)	1.2489(7)

[a] Estimated uncertainties, given in parentheses, refer to the least significant digit(s) of the tabulated value.
[b] An independent fit of $\dot{\omega}$ for B yields this value, consistent with the much more precise result for A.

in fact be calculated, and has the virtue of being equal to the mass ratio M_A/M_B to first post-Newtonian order in *all* theories of gravity (Damour & Schäfer 1988; Damour & Taylor 1992).

Thanks to the uniqueness of the Double Pulsar we are hence able to obtain 5 + 1 − 2 = 4 separate tests of GR through pulsar timing observations (and an additional, fifth, test through the measurement of geodetic precession, see §4.3).

The confluence of these parameters in GR is illustrated in the mass-mass diagram of Figure 2 where, in the zoomed inset, we can see that these constraints meet in a single small area, proving that GR is correct at least at the 99.95% level.

To arrive at this number Kramer et al. (2006) considered the two most precisely measured PK parameters, $\dot{\omega}$ and s, and the theory-independent R. Using the measurement and the error ranges on $\dot{\omega}$ and R, and taking into account the uncertainty on the mass function of pulsar B implied by the uncertainty in R, Monte Carlo trials provided histograms of the most likely values for M_A and M_B within GR. These mass distributions were then used to make predictions, again assuming GR, for the value of s, along with the values of r, γ and $\dot{P}_b$. Each of these predictions agrees very well with the corresponding measured value (see Table 2). Specifically, the predicted and measured values of s match to within 0.05%, making this comparison the most precise test of GR in strong gravitational fields.

Table 2. Data taken from Kramer et al. (2006). Values are derived from the measured mass ratio R and advance of periastron$\dot{\omega}$. Estimated uncertainties, given in parentheses, refer to the least significant digit(s) of the tabulated value.

PK parameter	Observed	GR expectation	Ratio
$\dot{P}_b$	1.252(17)	1.24787(13)	1.003(14)
γ (ms)	0.3856(26)	0.38418(22)	1.0036(68)
s	0.99974(−39,+16)	0.99987(−48,+13)	0.99987(50)
$r(\mu s)$	6.21(33)	6.153(26)	1.009(55)

It is important to point out the extremely good agreement of the measured $\dot{P}_b$ with its GR-predicted value, not only because it reached a 1.4% precision in under three years of observations (Kramer et al. 2006) (compared to more than a decade for the Nobel prize pulsar B1913+16; Taylor & Weisberg 1989), but, most importantly, because the corrections to the observed value required to account for the acceleration of the binary relative to the Solar System barycenter (Damour & Taylor 1991) are very small (Kramer et al. 2006).

This is in contrast to the situation for other double neutron star systems for which this parameter is measured precisely: in particular for PSR B1913+16 the uncertainties in the Galactic acceleration limit the usefulness of the $\dot{P}_b$ GR test (Damour & Taylor 1991; Weisberg & Taylor 2005), while for PSR B1534+12 (Stairs et al. 2002) the poorly known pulsar distance results in a large uncertainty in the Shklovskii correction due to the changing Doppler effects arising from transverse motion (Shklovskii 1970). For J0737−3039A/B, considering the most precise distance

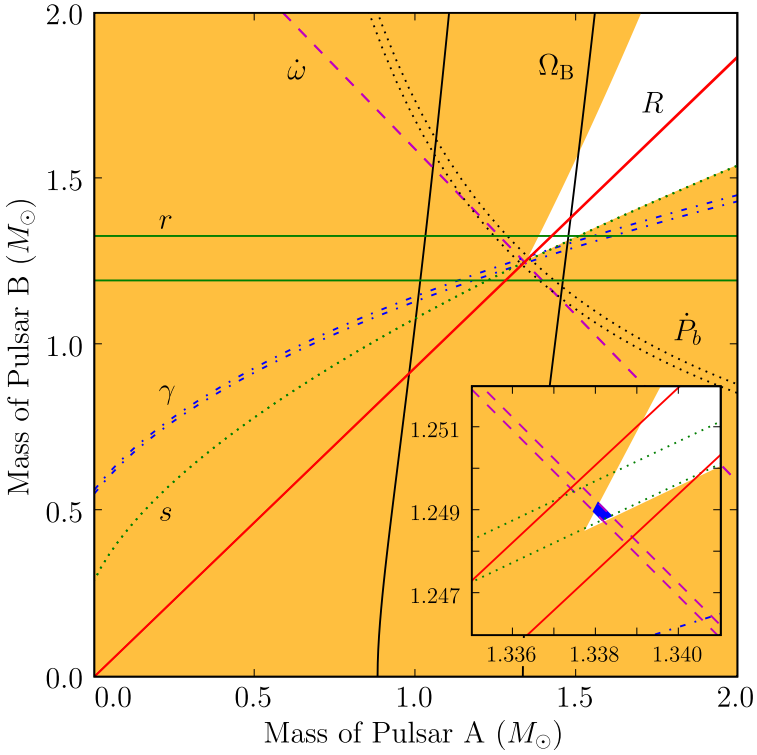

Figure 2. Mass-mass diagram of the Double Pulsar, summarizing the observational constraints on the masses M_A and M_B. The orange regions are those that are excluded by the Keplerian mass functions of the two pulsars. The other constraints are shown as pairs of lines enclosing permitted regions as predicted by general relativity: the measurement of the advance of periastron $\dot{\omega}$ (dashed purple line), the measurement of the mass ratio $R \equiv M_A/M_B = x_B/x_A$ (solid red line), the measurement of the gravitational-redshift/time-dilation parameter γ (dashed-dotted blue line), the measurement of the rate of the Shapiro delay r (solid green line) and shape of the Shapiro delay s (dotted green line), and the measurement of the orbital decay $\dot{P}_b$ (dashed-double-dotted black line), the measurement of the relativistic spin precession (solid black lines; see §4.3). Inset: an enlarged view of the square encompassing the intersection of the tightest constraints. The permitted regions are those between the pairs of parallel lines. The light-blue area is compatible with all constraints.

measurement available so far (Deller et al. 2009), the complete set of corrections adds up to only 0.01% of the measured value of $\dot{P}_b$ (Deller et al. 2009).

2.2 Alternative theories

A test of a theory of gravity as described above using binary pulsars can only falsify a given theory. Hence, even though there is an excellent agreement of the timing results with the predictions of general relativity, it is still possible that the correct underlying theory of gravity deviates from GR. In particular the phenomena interpreted as "Dark Matter" and "Dark Energy" have created renewed doubts as to whether the corresponding observations point towards a deviation from GR. A large variety of alternative theories exists, but most of them are not developed sufficiently well to make predictions that can be tested experimentally. In particular a most important test for every theory is its prediction for gravitational wave emission, an observation that so far can only be tested with binary pulsars. Indeed, most alternative theories predict a violation of the Strong Equivalence Principle (SEP), for instance due to the existence of scalar fields and resulting self-field effects that depend on the composition of the massive object. As a result, in a binary system, the orbital decay would be modified, as both components would fall differently in the external field of the companion and the Galaxy. The result would be the emission of gravitational *dipolar* radiation, which can be expected to be larger in amplitude compared to GR's quadrupolar emission. The result would be a measured $\dot{P}_b$ value that deviates significantly from GR's prediction. In general, a double neutron star system like the Double Pulsar has only limited power for such a test, because the fact that binary systems consists of the same type of object (i.e. two neutron stars) creates only a small amount of dipolar radiation as the differences in coupling to the scalar field is small. In contrast, a pulsar-white dwarf system, where both binary components are vastly different in their composition, is much more useful (Freire et al. 2012; Antoniadis et al. 2013). However, the precision of the measurements of $\dot{P}_b$ for PSR J0737−3039A/B is so good, that the observations help ruling out (Kramer et al. in prep.) a large fraction of the best developed class of alternative theories, namely tensor-scalar theories (Damour & Esposito-Farese 1996).

3. Double neutron stars coalescence rate and gravitational wave detections

The merger of two neutron stars in a binary system, according to general relativity, should produce a burst of gravitational waves detectable by ground based laser interferometers such as LIGO (Abramovici et al. 1992) or VIRGO (Bradaschia et al. 1991). In order to predict whether such an event is likely to be detected by current generation instruments in a reasonable time span, it is necessary to reliably estimate the rate of double neutron star (DNS) merger events in our Galaxy (and, by extrapolation, in the close Universe).

These estimates are usually obtained using two different methods. One, purely theoretical, is based on models of binary evolution, while the other, more empirical, is based on the physical properties of the known close DNS binaries in the Galactic field and modeling of radio pulsar survey selection effects (see e.g. Kalogera et al. 2001).

Among the handful of DNS known to date in the field of our Galaxy, only three (B1913+16; Taylor & Weisberg 1989, B1534+12; Stairs et al. 2002 and the Double Pulsar) will coalesce within a Hubble time, and will therefore affect coalescence rate estimates. With a merging time of only 85 Myr, the Double Pulsar is by far the most relativistic of the known population. Original estimates, based on the small distance to and the short predicted life time of this binary, argued that the Galactic volume per double-pulsar-like system should be quite small, and therefore that there could be large numbers of similar systems in the Galaxy. Its discovery therefore immediately boosted the predicted merger rate by almost an order of magnitude (Burgay et al. 2003; Kalogera et al. 2004b; Lorimer et al. 2007). More recent work has accounted for the beaming geometries of A and B (O'Shaughnessy & Kim 2010; Kim et al. 2013), and assumes a luminosity function for the pulsar population so that the proximity of the Double Pulsar no longer influences the rates. The predicted merger rates using these estimates (see Figure 3) are decreased from the original ones, but still suggest that the current versions of ground based gravitational wave detectors could detect one or more inspirals over the duration of the experiments.

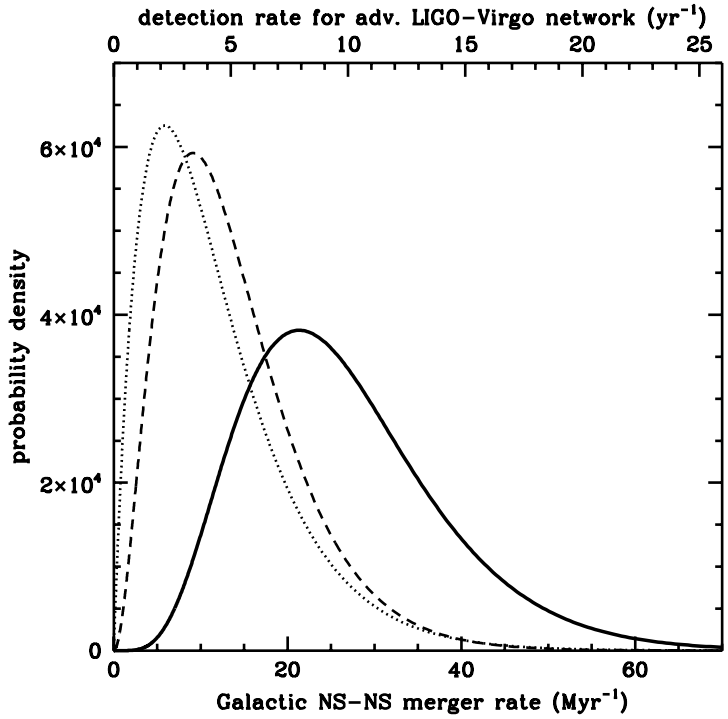

Figure 3. Total probability density function (PDF) of the DNS merger rate (solid curve) overlaid with individual PDFs obtained from PSR B1916+13 (dotted) and the Double Pulsar (short dashed). Based on the reference model from Kim et al. (2013), the Galactic DNS merger rate is most likely to be 21 Myr^{-1} . The corresponding GW detection rate for the advanced ground-based GW detectors is 8 yr^{-1}.

4. Mutual interactions in the Double Pulsar

One of the observational aspects that makes the J0737−3039A/B system so unique is the presence of the pulsed signals from both pulsar A and pulsar B. As the spin-down energy loss rate of A is over 3000 times that of B, the wind from A influences the emission of B in several ways. In addition, the orbit is almost edge-on (see Table 1), leading to the observation of eclipses from pulsar B. These interactions between the beam of A with the magnetosphere of B provides insights into pulsar emission mechanisms, magnetosheric properties and plasma physics.

4.1 Pulse shape and flux variations in B

The radio emission of pulsar B is unusual in several ways, including the presence of dramatic profile and flux variations, both on orbital (minutes–hours) and longer, secular (∼years) timescales. The latter of these has resulted in B being undetectable since 2008. In addition, we observe drifting-like features in its single pulses due to the influence of pulsar A.

4.1.1 *Variations over an orbital timescale*

Pulsar B was not immediately detected along with pulsar A in the original search data taken for the Parkes High-latitude survey because its flux density varies greatly along the orbit (Lyne et al. 2004), and the original discovery observation occurred during a 'weak' phase. When B was eventually discovered, roughly six months after A, it was found that it was clearly visible only in two subsections of the orbit, one (bright-phase 1, or bp1) covering the orbital phase range $\sim 190^\circ - 235^\circ$, and the other (bp2) covering the range $\sim 260^\circ - 300^\circ$ (see Figure 4), while in the rest of the orbit it was very faint or completely undetectable.

Together with the flux variations, there is also a clear variability with orbital phase in the shape of the pulse profile. For instance, in the center panel of Figure 4, where each vertical stripe represents the average profile in 1 orbital degree chunks, one can clearly see that in bp1 the main (darker) pulse is much more prominent than its precursor, while in bp2 a double peaked profile with more similar maxima, both fainter than the peak of bp1, can be seen.

Lyutikov (2005) proposed that the observed orbital modulations of flux density and pulse shape are due to distortions of pulsar B's magnetosphere by pulsar A's wind. Pulsar B, in this model, would be intrinsically bright at all orbital phases, but would normally point away from Earth, with its radiation beam getting distorted and pushed towards our line of sight at only two orbital phases. Lyutikov's model, later refined to take into account variations on longer timescales (see §4.1.2; Lomiashvili & Lyutikov 2014) accurately reproduces both the extent and the location of the bright phases while also accounting for the profile variations. These, in fact, would be due to the fact that at different orbital phases the line of sight crosses the emission region along different paths.

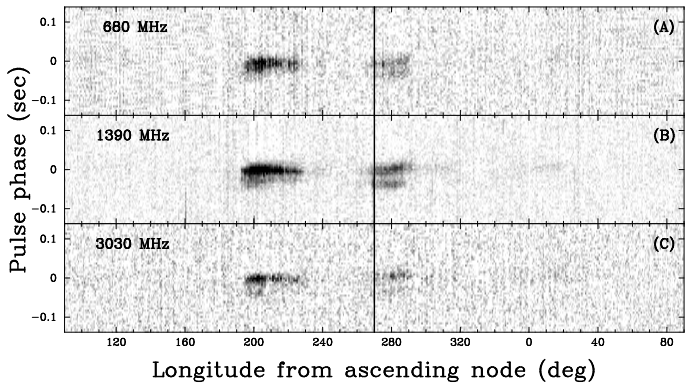

Figure 4. Light curve of pulsar B at three different frequencies as a function of orbital phase relative to the ascending node. Each panel shows B's intensity over a phase range of 0.1 of pulsar rotational period centered on the pulsed emission. Panels a, b, and c present observations at 680 MHz, 1390 MHz, and 3030 MHz. The vertical line at orbital phase 270° represents the longitude of the inferior conjunction of B shortly after the discovery of the Double Pulsar.

4.1.2 *Variations over a secular timescale*

The different panels of Figure 5 show the pattern of variations in flux and pulse shape of pulsar B at different epochs, from May 2003 to December 2004. It is clear that the position and extent of the bright phases are changing, with the centroid of both bp1 and bp2 moving towards higher longitudes and the duration of each shortening (Burgay et al. 2005; Perera et al. 2010).

At the same time, the shape and the intensity of the pulsed emission are observed to vary on long timescales, as can be seen in Figure 6, showing profiles for bp1 at 820 MHz at 12 different epochs spanning from 2003 to 2008, when pulsar B became undetectable.

In the Double Pulsar, secular variations in the geometry of the system occurring as a result of strong relativistic effects happen on a very short timescale. For pulsar B, the relativistic precession of the spin axis around the total angular momentum of the system (Damour & Ruffini 1974) and the periastron advance have periods of only 71 and 21 yr, a much shorter time span than for any other known binary pulsar. A change in the inclination of the spin axis due to precession leads to a change in the line of sight of an observer on Earth through the emission beam, resulting in an observed pulse shape variation. Also, since the orbital-scale variations of B's pulsed emission, according to the models described in §4.1, depend on the interaction between A's wind with B's magnetosphere, a change in the geometry due to both precession and periastron advance is expected to cause variations in the observed orbital-scale patterns, as the relative angle of A's wind and B's magnetosphere vary.

Through studying the shape of the profiles of pulsar B using more than five years of data taken with the Green Bank Telescope (GBT), Perera et al. (2010) were able to successfully model

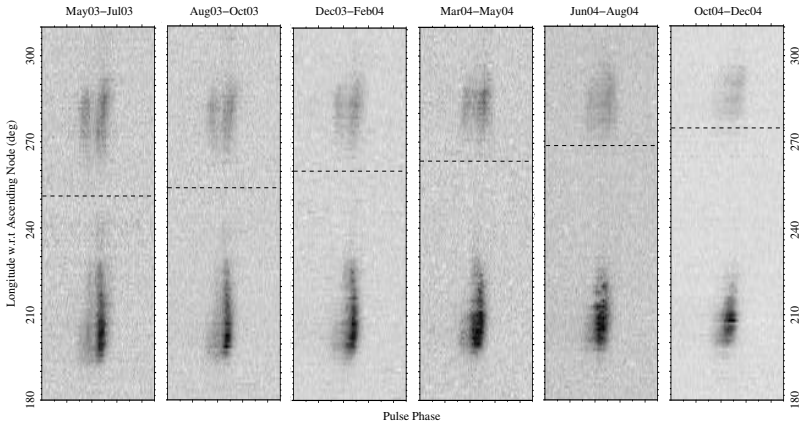

Figure 5. From Burgay et al. (2005): intensity of PSR J0737−3039B's pulse emission at 1390 MHz as a function of orbital longitude and pulse phase at six epochs. Only the longitude range 180 °-310 °, covering the two bright phases bp1 (lower) and bp2 (upper) and a pulse-phase window of 0.1 pulse periods centered on the pulse are shown. The dashed lines represent the longitude of periastron at each epoch.

the observed pulse shapes and variations, under the assumption that they are indeed caused by relativistic spin precession. A standard circular hollow-cone model for the emission beam, however, is not able to explain the observational properties well and yelds parameters for the geometry of B that are inconsistent with those obtained by Breton et al. (2008) (see §4.3). A much better fit and a consistent geometry are obtained by modeling the beam with an elliptical horseshoe, or partially filled, beam model. This model is able to account for the observed single- to double-peak pulse profile evolution and for the disappearance of radio emission in 2008.

With their model, Perera et al. (2010) also predicted that pulsar B will be again visible in ∼2035 (or, if the beam has a symmetric shape, within the next few months[1]). Using a more refined three dimensional model, Perera et al. (2012) were able to obtain a more realistic model for the beam shape. Their best fit resulted in an elliptical hollow-cone beam and in a geometry for pulsar B still fully compatible with the previous results, but providing an estimate of the reappearance of pulsar B for the year 2024.

By taking advantage of the now well determined geometry for pulsar B, Perera et al. (2012) were also able to develop a model of the wind-distorted magnetosphere of pulsar B and to determine the pulsar emission height. The height of emission varies across the orbit and with time, but is consistent with emission heights estimates for other pulsars through different methods. This is consistent with the theory of Lyutikov (2005) that B is a normal pulsar which is being perturbed by the wind of A.

As mentioned above, relativistic spin precession, resulting in a changing impact angle be-

[1] At the time of writing (September 2014)

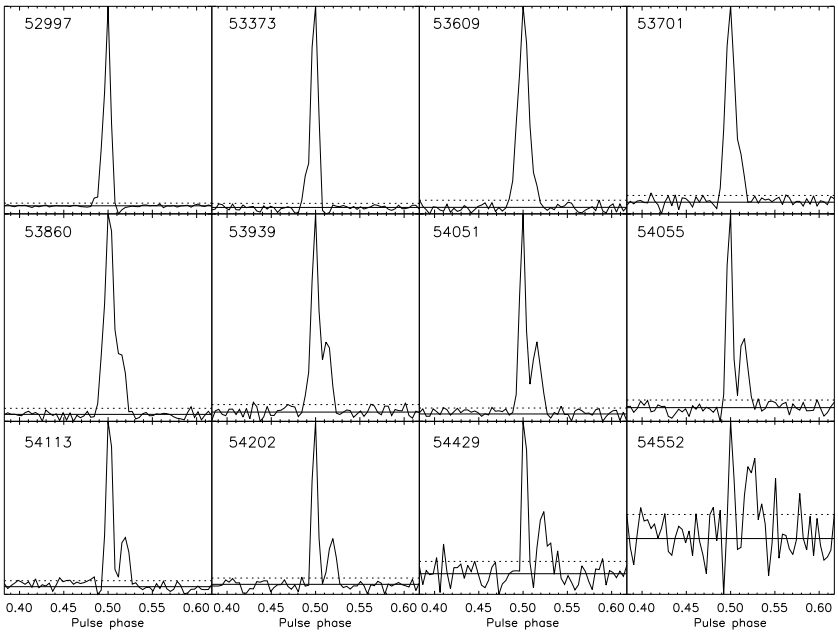

Figure 6. From Perera et al. (2010): pulse profiles for B's first bright phase at 12 different epochs over a span of over four years (the MJD is indicated on each profile). All data have been observed at a frequency of 820 MHz with the Green Bank Telescope. Each profile covers 20 minutes of orbital longitude (from 185 ° to 235 °) and is represented with 256 time bins The horizontal solid and dotted lines show the baseline, or off-pulse mean, of the profile and the corresponding standard deviation of the off-peak region, respectively.

tween B's magnetosphere and A's wind, can also be invoked to account for the observed variations of the location and extent of bright emission phases. By numerically modeling the distortions of the magnetosphere of pulsar B by the magnetized wind from pulsar A, including effects of magnetic reconnection and of the relativistic spin precession, Lomiashvili & Lyutikov (2014) successfully reproduce orbital variations and secular evolution of the profile of B, as well as the subpulse drift observed in the single pulses of pulsar A at specific orbital phases (see §4.2). With their model Lomiashvili & Lyutikov (2014) put forward again a horseshoe shaped radio beam for B, but in this case the prediction for reappearence of the pulsed emission is either 2034 or 2043, for a two-pole emission configuration, or 2066 for a single-pole.

4.2 Drifting pulses in pulsar B

Another remarkable feature of B's emission (Fig. 7) are 'drifting' features (McLaughlin et al. 2004b) similar to the drifting subpulses seen in many long-period pulsars, but with spacing *exactly* equal to the spin period of A, implying that the driftbands are produced by A's electromagnetic radiation. The driftbands can be seen only in bp1, where the radiation from A meets our line

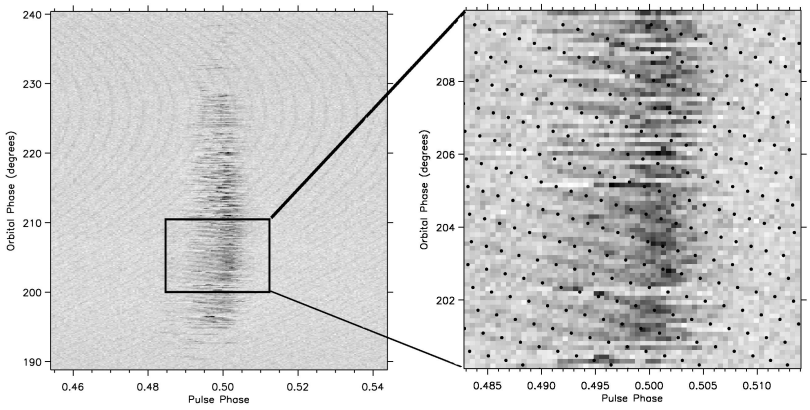

Figure 7. Single pulses of pulsar B at 820 MHz for orbital phases 190 – 240 ° as measured in December 2003. Only 10% of the pulse period of B is shown. Single pulses from both pulse profile components of A can be seen in the background (as curved stripes). At orbital phase ∼225 °, differential Doppler shifts from the orbital motion result in harmonically related apparent pulse periods. Drifting features are present in most of these data, but are particularly obvious from orbital phases ∼195 - 210 °. An expanded view of this region is shown on the right, where dots denote the arrival of emission from an arbitrary rotational phase of A at the center of B; the emission is retarded by the propagation time across the orbit.

of sight to B from the side, suggesting that that they are generated high in the magnetosphere. This is the first example of pulsar emission being triggered externally and, as such, could offer valuable insights into the pulsar emission process.

Freire et al. (2009) demonstrated that one could use measurements of the 'response delay', or the time difference between the arrival of a B driftband and the closest A radio pulse, to estimate several physical parameters describing the system. These include the offset angle between A's radio and electromagnetic beams, the height in B's magnetosphere at which the driftbands originate, and the sense of rotation of A with respect to the orbital rotation. The offset angle and the sense of rotation have not been measured through any means for any pulsar, making this a unique opportunity. While estimates for emission heights for several pulsars have been made, and a minimum and maximum emission height has been estimated for B from the geometry and magnetospheric modeling (Perera et al. 2012), this would represent the first actual measurement of the emission height for any pulsar. Liang et al. (2014) suggested a complementary method which relies on using frequencies instead of arrival times; this may simplify the analysis.

4.3 Eclipses of A by B

At superior conjunction pulsar A's signal is characterized by a short, ∼30 s, eclipse whose duration is modestly dependent on the observing frequency (Kaspi et al. 2004). Given the size and the

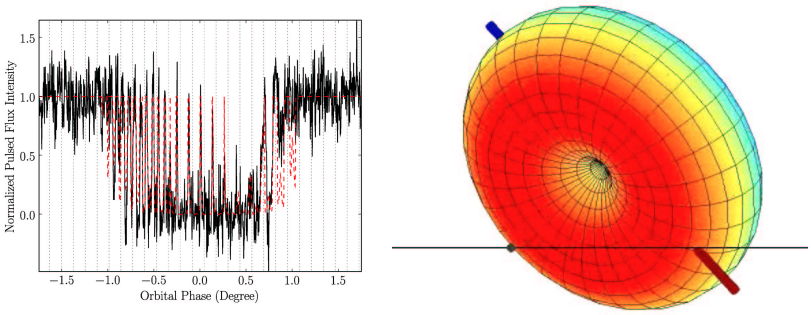

Figure 8. Left: average eclipse light-curve of pulsar A at 820 MHz obtained with eight eclipses over a five-day period around April 11, 2007 (black solid line) along with a model eclipse profile (red dashed line). Dashed black lines denote the time of arrival of B's pulses at A. Near orbital phase 0.0 the spikes are separated by the spin period of pulsar B, while at eclipse ingress at half B's period (Breton et al. 2008). Right: geometric model for B's magnetosphere eclipsing A (black circle) along its orbit (horizontal line).

inclination of the orbit, measured through the parameter $s \equiv sini = 0.99974$ of the Shapiro delay, we can infer that the eclipse region extends to $\sim 1.5 \times 10^7$ m. A close inspection of the eclipsed region shows that the emission of pulsar A, plotted in black on the left side of Figure 8, is not continuously eclipsed, but that it is modulated at either the spin period of pulsar B (near phase 0) or half this value (close to eclipse ingress; McLaughlin et al. 2004b), with the deepest part of the eclipse corresponding to when the magnetic pole of B points towards A. This implies that the eclipsing material must be corotating with pulsar B.

The most likely mechanism for an efficient absorption of radio waves over a wide range of frequencies is synchrotron resonance with relativistic electrons. Lyutikov & Thompson 2005 and Rafikov & Goldreich 2005 propose that this absorbing plasma corotates with pulsar B and is confined within the closed field lines of its magnetosphere, truncated by the relativistic wind emitted by pulsar A.

To explain in detail the modulation of pulsar A's signal at B's period, Lyutikov & Thompson (2005), and later Breton et al. (2008), produced a geometrical model of the Double Pulsar, including pulsar B's magnetosphere with a dipolar geometry (see of Fig. 8), through which it is possible to simulate pulsar A's signal in the eclipsed region. The (impressively accurate) best fit model, shown with a red dashed line in the left plot of Fig. 8, is obtained using the geometrical parameters listed in Table 3 (Breton et al. 2008).

The success of the model implies that pulsar B's magnetosphere is accurately described as predominantly dipolar; a pure quadrupole, for instance, would not reproduce the observed light curves (Breton et al. 2008). Although the model does not exclude the presence of higher-order multipole components close to the neutron star surface, this model, supports the long-standing assumption that pulsars have mainly dipolar magnetic fields far from their surface (Lyutikov & Thompson 2005; Breton et al. 2008).

Table 3. Geometrical parameters (and their graphical representation) of pulsar B derived from the eclipse model fitting. Here, α is the angle between the magnetic axis μ and rotational axis Ω, θ is the the colatitude of the spin axis with respect to the total angular momentum of the system (which, in this almost edge-on system, is very close to the plane of the sky, perpendicular to the line of sight), and ϕ is the longitude of the spin axis. The epoch of $\phi = \phi_0$ is May 2, 2006 (MJD 53857).

Angle	Mean	Median	68.2% Confidence
α_0	70.92 °	70.94 °	[70.49, 71.31] °
θ_0	130.02 °	130.02 °	[129.58, 130.44] °
ϕ_0	51.21 °	51.20 °	[50.39, 52.03] °

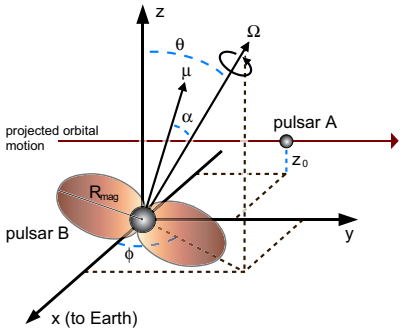

Since the exact pattern of the observed modulation depends on the relative geometry of pulsar B's magnetosphere with respect to pulsar A, relativistic spin precession is expected to modify the eclipse's shape in time. In particular, while the angles α and θ (see geometrical representation of B in the figure to the right of Table 3) should remain fixed, ϕ should change in time causing modifications in the observed light curves. By applying the fit to eclipses obtained over a four year period, Breton et al. (2008) showed that indeed only ϕ changed significantly with time and their results provided the first direct measurement of the relativistic spin precession for pulsar B, $\Omega_B = 4.77^{+0.66}_{-65}$ ° yr^{-1}. This value is in agreement, within an uncertainty of 13%, with the precession rate predicted by GR, $\Omega_{B,GR} = 5.0737 \pm 0.0007$ ° yr^{-1} (see Figure 2). This unique measurement increases the tests for GR in the Double Pulsar to a total of five!

4.4 Pulse shape of pulsar A

If the spin axis of a pulsar in a binary system is not parallel to the total angular momentum axis, relativistic spin precession should result, as demonstrated for pulsar B, in an observed change in the shape of the pulse profiles. Analysis of three (Manchester et al. 2005) and seven (Ferdman et al. 2013) years of data on pulsar A show no evidence for variations in the pulse shape (see Figure 9), leading to the conclusion that pulsar A's spin axis is indeed closely aligned with the orbital angular momentum vector.

This result is very important, on one hand because constraining the geometry for both A and B is crucial for some of the new measurements we will be able to perform in the next few years (see §5), and on the other because, with an unchanging pulse profile due to the lack of relativistic spin precession, the timing of A benefits from a stable pulse shape and constant phase reference, allowing us to continually increase the precision of the timing model.

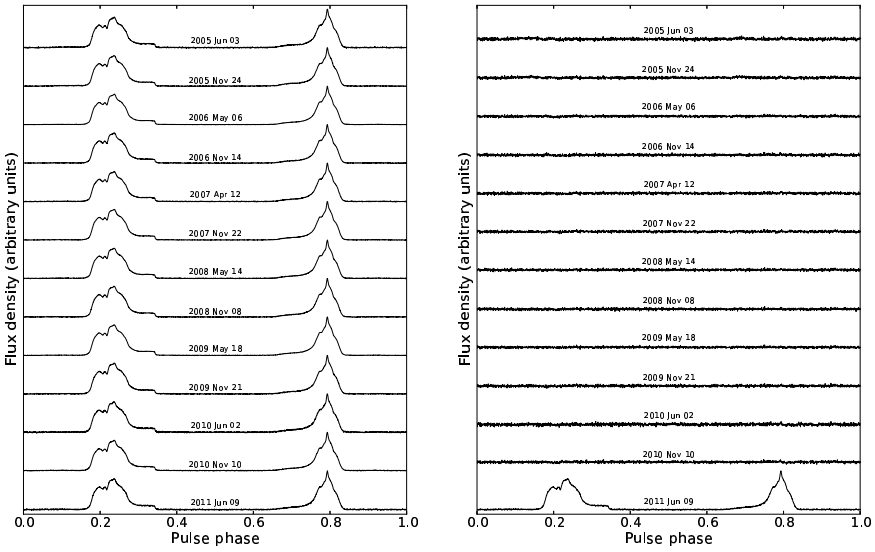

Figure 9. From Ferdman et al. (2013): integrated pulse profiles (left) and difference profile residuals (right) over nearly 7 years of GBT observations. Each subplot is labeled with the central date of the given epoch. The difference profiles in the right-hand panel are plotted at twice the vertical scale of the left-hand panel.

5. Future

Observations of the Double Pulsar system now span over a whole decade and in particular for about half the period of precession of the longitude of periastron. As a result, timing parameters of pulsar A can be measured with superb accuracy. This allows not only for the most precise measurement of the orbital decay rate of any binary system (and hence the best evidence for the existence of gravitatinal wave emission thus far), but it also allows unprecedented tests of alternative theories of gravity. Besides testing classes of theories, such as tensor-scalar theories, particular effects such as the existence of preferred frame effects (Wex & Kramer 2007) can also be probed uniquely. Continued observations will provide further constraints and continuously improving precision for such tests, in particular when pulsar B reappears. One of the important goals for the future is, however, the measurement of the moment-of-interia of pulsar A. This is possible by extracting the spin-contribution to the observed value of the periastron advance. While it will be difficult to isolate this effect by determining two PK parameters (other than $\dot{\omega}$) with sufficient precison, it will provide one of the most valuable constraints on discussed equations-of-state of super-dense matter. Observations with future telescopes like the Square Kilometre Array (SKA) will lead to such measurements. Indeed, with the SKA, the J0737−3039A/B system will continue to be one of the richest astrophysical laboratories ever found, allowing us to study a wide range of physics and astrophysics in a compact nearby binary system. The fun continues.

Acknowledgements

We would like to thank all our collaborators that in the past decade worked with us to explore the many wonders of the Double Pulsar.

References

Abramovici A., Althouse W. E., Drever R. W. P., Gursel Y., Kawamura S., Raab F. J., Shoemaker D., Sievers L., Spero R. E., Thorne K. S., Vogt R. E., Weiss R., Whitcomb S. E., Zucker M. E., 1992, Science, 256, 325

Antoniadis J., Freire P. C. C., Wex N., Tauris T. M., Lynch R. S., van Kerkwijk M. H., Kramer M., Bassa C., Dhillon V. S., Driebe T., Hessels J. W. T., Kaspi V. M., Kondratiev V. I., Langer N., Marsh T. R., McLaughlin M. A., Pennucci T. T., Ransom S. M., Stairs I. H., van Leeuwen J., Verbiest J. P. W., Whelan D. G., 2013, Science, 340, 448

Bradaschia C., Calloni E., Cobal M., del Fabbro R., di Virgilio A., Giazotto A., Kautzky H., Montelatici V., Passuello D., Velloso W., Barone F., di Fiore L., Milano L., Russo G., Solimeno S., Gammaitoni L., Marchesoni E., Santucci S., Brillet A., Davier M., Durand E., Hello P., Ivanov D., Lesimple M., Man C. N., Marraud A., Pham Tu M., Vinet J. Y., Boccara C., Roger J. P., Colas J., Girard M., Yvert M., Massonetr L., Mours B., Wingerter I., 1991, in McClelland D. E., Bachor H.-A., eds, Gravitational Astronomy: Instrument Design and Astrophysical Prospects Interferometric detection of gravitational waves: the VIRGO project. p. 110

Breton R. P., Kaspi V. M., Kramer M., McLaughlin M. A., Lyutikov M., Ransom S. M., Stairs I. H., Ferdman R. D., Camilo F., Possenti A., 2008, Science, 321, 104

Burgay M., D'Amico N., Possenti A., Manchester R. N., Lyne A. G., Joshi B. C., McLaughlin M. A., Kramer M., Sarkissian J. M., Camilo F., Kalogera V., Kim C., Lorimer D. R., 2003, Nature, 426, 531

Burgay M., Joshi B. C., D'Amico N., Possenti A., Lyne A. G., Manchester R. N., McLaughlin M. A., Kramer M., Camilo F., Freire P. C. C., 2006, MNRAS, 368, 283

Burgay M., Possenti A., Manchester R. N., Kramer M., McLaughlin M. A., Lorimer D. R., Stairs I. H., Joshi B. C., Lyne A. G., Camilo F., D'Amico N., Freire P. C. C., Sarkissian J. M., Hotan A. W., Hobbs G. B., 2005, ApJ, 624, L113

Cordes J. M., Lazio T. J. W., 2002, arXiv:astro-ph/020715

Damour T., Deruelle N., 1986, Ann. Inst. H. Poincaré (Physique Théorique), 44, 263

Damour T., Esposito-Farese G., 1996, Phys. Rev. D, 54, 1474

Damour T., Ruffini R., 1974, Academie des Sciences Paris Comptes Rendus Ser. Scie. Math., 279, 971

Damour T., Schäfer G., 1988, Nuovo Cim., 101, 127

Damour T., Taylor J. H., 1991, ApJ, 366, 501

Damour T., Taylor J. H., 1992, Phys. Rev. D, 45, 1840

Deller A. T., Bailes M., Tingay S. J., 2009, Science, 323, 1327

Ferdman R. D., Stairs I. H., Kramer M., Breton R. P., McLaughlin M. A., Freire P. C. C., Possenti A., Stappers B. W., Kaspi V. M., Manchester R. N., Lyne A. G., 2013, ApJ, 767, 85

Freire P. C. C., Wex N., Esposito-Farèse G., Verbiest J. P. W., Bailes M., Jacoby B. A., Kramer M., Stairs I. H., Antoniadis J., Janssen G. H., 2012, MNRAS, 423, 3328

Freire P. C. C., Wex N., Kramer M., Lorimer D. R., McLaughlin M. A., Stairs I. H., Rosen R., Lyne A. G., 2009, MNRAS, 396, 1764

Kalogera V., Kim C., Lorimer D. R., Burgay M., D'Amico N., Possenti A., Manchester R. N., Lyne A. G., Joshi B. C., McLaughlin M. A., Kramer M., Sarkissian J. M., Camilo F., 2004a, ApJ, 614, L137

Kalogera V., Kim C., Lorimer D. R., Burgay M., D'Amico N., Possenti A., Manchester R. N., Lyne A. G., Joshi B. C., McLaughlin M. A., Kramer M., Sarkissian J. M., Camilo F., 2004b, ApJ, 601, L179
Kalogera V., Narayan R., Spergel D. N., Taylor J. H., 2001, ApJ, 556, 340
Kaspi V. M., Ransom S. M., Backer D. C., Ramachandran R., Demorest P., Arons J., Spitkovsky A., 2004, ApJ, 613, L137
Kim C., Bhakthi Pranama Perera B., McLaughlin M. A., 2013, ArXiv e-prints
Kramer M., Stairs I. H., Manchester R. N., McLaughlin M. A., Lyne A. G., Ferdman R. D., Burgay M., Lorimer D. R., Possenti A., D'Amico N., Sarkissian J. M., Hobbs G. B., Reynolds J. E., Freire P. C. C., Camilo F., 2006, Science, 314, 97
Liang Z.-X., Liang Y., Weisberg J. M., 2014, MNRAS, 439, 3712
Lomiashvili D., Lyutikov M., 2014, MNRAS, 441, 690
Lorimer D. R., Freire P. C. C., Stairs I. H., Kramer M., McLaughlin M. A., Burgay M., Thorsett S. E., Dewey R. J., Lyne A. G., Manchester R. N., D'Amico N., Possenti A., Joshi B. C., 2007, MNRAS, 379, 1217
Lorimer D. R., Kramer M., 2005, Handbook of Pulsar Astronomy. Cambridge University Press
Lyne A. G., Burgay M., Kramer M., Possenti A., Manchester R. N., Camilo F., McLaughlin M. A., Lorimer D. R., D'Amico N., Joshi B. C., Reynolds J., Freire P. C. C., 2004, Science, 303, 1153
Lyutikov M., 2005, MNRAS, 362, 1078
Lyutikov M., Thompson C., 2005, ApJ, 634, 1223
Manchester R. N., Kramer M., Possenti A., Lyne A. G., Burgay M., Stairs I. H., Hotan A. W., McLaughlin M. A., Lorimer D. R., Hobbs G. B., Sarkissian J. M., D'Amico N., Camilo F., Joshi B. C., Freire P. C. C., 2005, ApJ, 621, L49
McLaughlin M. A., Kramer M., Lyne A. G., Lorimer D. R., Stairs I. H., Possenti A., Manchester R. N., Freire P. C. C., Joshi B. C., Burgay M., Camilo F., D'Amico N., 2004a, ApJ, 613, L57
McLaughlin M. A., Lyne A. G., Lorimer D. R., Possenti A., Manchester R. N., Camilo F., Stairs I. H., Kramer M., Burgay M., D'Amico N., Freire P. C. C., Joshi B. C., Bhat N. D. R., 2004b, ApJ, 616, L131
O'Shaughnessy R., Kim C., 2010, ApJ, 715, 230
Perera B. B. P., Lomiashvili D., Gourgouliatos K. N., McLaughlin M. A., Lyutikov M., 2012, ApJ, 750, 130
Perera B. B. P., McLaughlin M. A., Kramer M., Stairs I. H., Ferdman R. D., Freire P. C. C., Possenti A., Breton R. P., Manchester R. N., Burgay M., Lyne A. G., Camilo F., 2010, ApJ, 721, 1193
Rafikov R. R., Goldreich P., 2005, ApJ, 631, 488
Shapiro I. I., 1964, Phys. Rev. Lett., 13, 789
Shklovskii I. S., 1970, Sov. Astron., 13, 562
Stairs I. H., Thorsett S. E., Taylor J. H., Wolszczan A., 2002, ApJ, 581, 501
Taylor J. H., Weisberg J. M., 1989, ApJ, 345, 434
Weisberg J. M., Taylor J. H., 2005, in Rasio F., Stairs I. H., eds, Binary Radio Pulsars The Relativistic Binary Pulsar B1913+16. Astronomical Society of the Pacific, San Francisco, pp 25–31
Wex N., Kramer M., 2007, MNRAS, 380, 455